

Article

MK-1 Orthopyroxene—A New Potential Reference Material for In-Situ Microanalysis

Lihui Jia ^{1,*}, Qian Mao ¹, Bin Su ¹, Shitou Wu ¹, Liangliang Huang ¹, Jianguan Yuan ¹, Di Zhang ¹
and Yi Chen ^{1,2,*}

¹ State Key Laboratory of Lithospheric Evolution, Institute of Geology and Geophysics, Chinese Academy of Sciences, Beijing 100029, China; maoqian@mail.iggcas.ac.cn (Q.M.); subin@mail.iggcas.ac.cn (B.S.); shitou.wu@mail.iggcas.ac.cn (S.W.); huangll@mail.iggcas.ac.cn (L.H.); yuanjy@mail.iggcas.ac.cn (J.Y.); zhangdi@mail.iggcas.ac.cn (D.Z.)

² University of Chinese Academy of Sciences, Beijing 100029, China

* Correspondence: jialihui@mail.iggcas.ac.cn (L.J.); chenyi@mail.iggcas.ac.cn (Y.C.);
Tel.: +86-010-8299-8577 (L.J.); +86-010-8299-8534 (Y.C.)

Abstract: Orthopyroxene, an important phase in mantle-derived rocks, has become a powerful tool to unravel mantle nature and magma processes. However, the applications have been hindered by the lag in the development of analytical techniques, such as shortage of reference materials. Orthopyroxene grains derived from an ultramafic intrusion at the Mogok metamorphic belt (Myanmar) were evaluated for the potential use of orthopyroxene as a reference material for in-situ microanalysis. Approximately 20 g of 0.5–3 mm pure orthopyroxene grains were separated under binocular microscope and analyzed using EPMA, LA-ICPMS, and bulk analytical methods (XRD, XRF, and solution-ICPMS) for major and trace elements at four institutions. Eleven core-to-rim profiles carried out using EPMA and twelve core-to-rim profiles determined using LA-ICPMS suggest that MK-1 orthopyroxene grains are sufficiently homogeneous, with RSD < ±2% (1σ) for major elements (Mg, Si, and Fe) and RSD < ±10% (1σ) for trace elements (Na, Al, Ca, Ti, Cr, Co, Zn, Ni, Mn, Sc, and V). In addition, the composition of MK-1 orthopyroxene was also measured by XRF and solution-ICPMS measurements in two different laboratories, to compare with the results measured using EPMA and LA-ICPMS. The results indicated a good agreement with RSE < ±2% (1σ) for major elements and RSE < ±5% (1σ) for most trace elements, except for Na (±9.73%) and Ti (±6.80%). In an overall assessment of these data, MK-1 orthopyroxene can be considered as a reference material for in-situ microanalysis, which would provide solid trace elements data for a better understanding of mantle source and magmatic evolution.

Keywords: MK-1; orthopyroxene; reference material; trace element; EPMA



Citation: Jia, L.; Mao, Q.; Su, B.; Wu, S.; Huang, L.; Yuan, J.; Zhang, D.; Chen, Y. MK-1 Orthopyroxene—A New Potential Reference Material for In-Situ Microanalysis. *Minerals* **2021**, *11*, 1321. <https://doi.org/10.3390/min11121321>

Academic Editor: William L. Griffin

Received: 9 October 2021

Accepted: 23 November 2021

Published: 26 November 2021

Publisher's Note: MDPI stays neutral with regard to jurisdictional claims in published maps and institutional affiliations.



Copyright: © 2021 by the authors. Licensee MDPI, Basel, Switzerland. This article is an open access article distributed under the terms and conditions of the Creative Commons Attribution (CC BY) license (<https://creativecommons.org/licenses/by/4.0/>).

1. Introduction

Orthopyroxene is the second most common phase in the upper mantle [1], and present as a phenocryst during crystallization of a wide range of melts, ranging from ultramafic boninite, to basalt, to andesite, rhyolite and granite [2–4]. Orthopyroxene is also an important cumulus phase in large layer intrusions [5] and ophiolites [6]. Despite its simple major element composition, orthopyroxene contains a number of petrogenetically significant trace elements, such as Al, Ca, Na, Ti, Cr, Zn, Co, and Ni [7,8]. Most trace elements of orthopyroxene (e.g., Ti, Cr, Ni, and Na) are used to calculate partition coefficient between orthopyroxene and silicate melts, which provide better constrained solutions to trace element models applied to magma genesis and differentiation [7]. In addition, crystal zoning patterns always occurred in orthopyroxene (e.g., Cr zoning [8] and Ti zoning [9]), which have been recognized as archives of magmatic processes such as fractional crystallization [10,11], magma replenishment [12,13], magma convection [14], and subsolidus equilibration [15,16]. Furthermore, the calculation of temperature and pressure also require

knowledge of the contents of trace elements (e.g., Al, Ti, Cr, Ca, and Na) in orthopyroxene, such as Opx-Cpx thermometer [17] or Grt-Opx barometer [18,19]. Consequently, trace elements in orthopyroxene have become powerful tools in unraveling the mantle nature and magma processes.

Despite its importance for petrological investigations, there is still a lack of well-characterized reference material available for validation of results obtained from high spatial resolution analysis of orthopyroxene. Early trace elements abundances were analyzed via laser ablation-inductively coupled plasma-mass spectrometry (LA-ICPMS), which utilized silicon as the internal standard and NIST SRM 610 glass as the calibrator. However, orthopyroxene that occurs as inclusion in basalt is small, and always exhibits a chemical zoning [10,12,15], which is hugely difficult in coordinating with the low spatial resolution weakness of LA-ICPMS. In addition, beam damage is another disadvantage in analyzing trace elements using LA-ICPMS. In recent years, trace element analysis using EPMA is becoming the backbone of numerous geochemical studies due to its high resolution, low-cost, and non-destructive characteristics [20–22], which requires a secondary reference for quality control and method validation purposes. Therefore, the development of a new orthopyroxene reference material is imperative.

In this study, we estimated the homogeneity of major and trace elements for an MK-1 orthopyroxene using EPMA, LA-ICP-MS, and bulk analytical methods (XRD, XRF, and solution ICP-MS). MK-1 orthopyroxene is well suited for trace element validation because it is significantly homogeneous and contains relatively high mass fractions of trace elements. Additionally, this paper attempts to improve the EPMA method to accurately analyze trace elements of orthopyroxene, and to effectively reduce the detection limits of trace elements. Our results would provide more solid data support for orthopyroxene compositions, and expand the applications of orthopyroxene in magmatic processes, temperature and pressure conditions, and lithospheric evolution.

2. Sample Description and Preparation

MK-1 orthopyroxenite from an ultramafic intrusion at the Mogok metamorphic belt (Myanmar) was selected as a suitable source for the new orthopyroxene reference material. The Mogok metamorphic belt exposes several narrow bodies of partially serpentinized ultramafic rocks that are aligned along minor faults connecting to the major E-W trending Momeik fault, which bounds the north side of the Mogok Tract. The ultramafic rocks consist of dunite, lherzolite, and orthopyroxenite. Dunite samples consist of olivine (>90 vol.%) and minor spinel, with an intergranular coating of lizardite. Lherzolite is composed of 45–60 vol.% olivine, 15–20 vol.% orthopyroxene, 10–15 vol.% clinopyroxene, 5–10 vol.% plagioclase and minor amounts of Cr-spinel and phlogopite, with lizardite serpentine coating all grain boundaries. Orthopyroxenite is composed of 60–80 vol.% cumulus euhedral orthopyroxene, 5–10 vol.% olivine, <10 vol.% clinopyroxene, and plagioclase, with minor amphibole and Cr-spinel. Orthopyroxene occurs as granular and poikilitic crystals, or as large oikocrysts enclosing fine-grained olivine. These rock types are cut by shear zones with the surfaces coated by shiny lizardite and veins of magnetite-rich spinel or snow-flake talc and lizardite.

The orthopyroxenite (20 kg) was crushed and sieved, and then approximately 20 g of orthopyroxene grains (0.5–3 mm) was hand-picked under a binocular microscope (Olympus SZ61, Tokyo, Japan). In order to find orthopyroxene suitable for use as mineral standards a large number of grains were investigated. The orthopyroxene grains were mounted in epoxy and polished for in-situ microanalysis. All grains were examined under reflected light microscopy (Olympus BX53, Tokyo, Japan) in order to identify possible microscopic mineral inclusions and mineral exsolutions. Those grains were then analyzed using scanning electron microscope (Nova Nano SEM 450, FEI Company, Hillsboro, OR, USA), where possible submicroscopic mineral inclusions and exsolutions could be detected. With this technique strong chemical zoning can also be identified. Orthopyroxenes appeared to be homogenous and free of inclusions based on optical inspection and SEM analysis were then

tested for elemental homogeneity by EPMA by conducting core-to-rim profiles through the grains. A preliminary electron microprobe investigation of 240 polished grains of orthopyroxene showed a fairly homogeneous composition for three major (Mg, Fe, and Si) and eleven trace elements (Al, Ca, Na, Ti, Cr, Zn, Co, Ni, Mn, V, and Sc).

3. Analytical Methods

3.1. Electron Probe Microanalysis (EPMA)

Major and trace elements in orthopyroxene were determined using EPMA of Cameca SXFive (Cameca Company, Paris, France) at the Institute of Geology and Geophysics, Chinese Academy of Sciences (IGGCAS). To pursue higher counts, better peak/back ratios, a higher acceleration voltage of 25 kV was adopted for both major and trace elements of olivine following literatures [20,21]. Two different analysis conditions were applied in one analytical setting. For major elements (Mg, Si, and Fe), a beam current of 60 nA and a short peak counting time of 10 s can meet the precision. Mg (K α), Si (K α), and Fe (K α) were simultaneously acquired in two WDS channels with diffracting crystals of TAP and LLiF, respectively. For trace elements (Na, Cr, Ti, V, Mn, Co, Ni, Zn, and Ca) in orthopyroxene, a higher beam current of 800 nA and a much longer peak count time of 120 s were applied to achieve receivable detection limits approaching to 10 $\mu\text{g g}^{-1}$, as well as an efficient measuring rate. WDS was set as: one TAP for Na (K α) and Al (K α), one LIF for Ni (K α) and Mn (K α), one LPET for Ca (K α) and Ti (K α), and one LLiF for Cr (K α), Co (K α), and Zn (K α). A large analyzing crystal (e.g., LLiF, LPET) is helpful in achieving higher counts and improving the analysis precision. The peak overlaps correction of Cr (K β) to Mn (K α) and Ti (K β) to V (K α) were applied. In order to keep Na X-ray intensity stable, Na was first tested on TAP crystal to reduce the heating time and thus beam damage. The natural minerals and synthetic oxides that were used for calibration are as follows: rhodonite (Si and Mn), apatite (Ca), rutile (Ti), albite (Na), FeS₂ (Fe), ZnS (Zn), Cr₂O₃ (Cr), Co (Co), Ni (Ni), and MgO (Mg). A program based on the ZAF procedure was used for data correction (CITIZAF) [23]. The detection limits were 5 $\mu\text{g g}^{-1}$ for Ti, 14 $\mu\text{g g}^{-1}$ for Mn, 12 $\mu\text{g g}^{-1}$ for Co, 23 $\mu\text{g g}^{-1}$ for Ni, 41 $\mu\text{g g}^{-1}$ for Zn, 6 $\mu\text{g g}^{-1}$ for Ca, 6 $\mu\text{g g}^{-1}$ for Al, and 11 $\mu\text{g g}^{-1}$ for Cr based on a 3 σ estimate of the measured background variance (Table 1).

Table 1. EPMA conditions applied for MK-1 orthopyroxene analysis.

| Element | Mg | Si | Fe | Na | Al | Ca | Ti | Cr | Co | Zn | Ni | Mn |
|----------------------------------|------------|------------|------------|------------|------------|------------|------------|------------|------------|------------|------------|------------|
| Acceleration voltage (kV) | 25 | 25 | 25 | 25 | 25 | 25 | 25 | 25 | 25 | 25 | 25 | 25 |
| Beam current (nA) | 60 | 60 | 60 | 800 | 800 | 800 | 800 | 800 | 800 | 800 | 800 | 800 |
| Crystal | TAP | TAP | LLiF | TAP | TAP | LPET | LPET | LLiF | LLiF | LLiF | LIF | LIF |
| Line | K α |
| Count time ^a (s) | 20 | 20 | 20 | 120 | 120 | 120 | 120 | 120 | 120 | 120 | 120 | 120 |
| Background time ^b (s) | 10 | 10 | 10 | 60 | 60 | 60 | 60 | 60 | 60 | 60 | 60 | 60 |
| DL ^c (ppm) | 146 | 113 | 141 | 15 | 6 | 6 | 5 | 11 | 12 | 41 | 23 | 14 |
| 3 σ ^d (ppm) | 2204 | 4302 | 616 | 13 | 5 | 7 | 4 | 9 | 10 | 183 | 38 | 17 |

^a Counting time on peak position. ^b Counting time on background position. ^c 3 σ detection limit. ^d 3 σ relative standard error based on counting statistics.

3.2. Laser Ablation Inductively Coupled Plasma-Mass Spectrometry (LA-ICPMS)

(IGGCAS) Trace element compositions of orthopyroxene were conducted using an Agilent 7500a quadrupole ICP-MS instrument (Agilent Technologies, Palo Alto, CA, USA) coupled with an Analyte G2 193 nm ArF excimer laser ablation system at the State Key Laboratory of Lithospheric Evolution, IGGCAS. The carrier gas, helium, went through the ablation cell, and argon was mixed downstream from the ablation cell. Prior to analysis, the Pulse/Analogue (P/A) factor of the detector was calibrated using a standard tuning solution. The spot size and frequency of the laser were set to 44 μm and 5 Hz, respectively. The laser energy density was $\sim 4.0 \text{ J/cm}^2$. All trace element determinations were carried out using time-resolved analysis in fast, peak jumping mode. Each spot analysis consisted of an

approximate 20 s background and a 60 s sample data acquisition. NIST SRM 610 reference glass was used as the calibration material, and ARM-1 [24] and BCR-2G were analyzed for data quality control. Silicon was used as an internal standard. The resulting data were reduced based on the GLITTER program [25]. For most trace elements ($>0.10 \text{ g g}^{-1}$), the accuracy is better than $\pm 10\%$ with analytical precision (1 RSD) of $\pm 10\%$. More details of the analytical procedures are provided in [26,27].

(SSATC) Trace element analyses of orthopyroxene were also performed using LA-ICPMS at Wuhan Sample Solution Analytical Technology Co., Ltd. (SSATC), Wuhan. The detailed operating conditions used for the laser ablation system and the ICP-MS instrument and data reduction are the same as description by [28]. Laser sampling was performed using a Geolas laser ablation system that consists of a COMPexPro 102 ArF excimer laser (wavelength of 193 nm and maximum energy of 200 mJ) and a MicroLas optical system. An Agilent 7900 ICP-MS instrument was used to acquire ion-signal intensities. Helium was applied as a carrier gas. Argon was used as the make-up gas and mixed with the carrier gas via a T-connector before entering the ICP. A “wire” signal smoothing device was included in this laser ablation system [29]. The spot size and frequency of the laser were set to 44 μm and 5 Hz, respectively. Trace element compositions of minerals were calibrated against various reference materials (BHVO-2G, BIR-1G, and BCR-2G) without using an internal standard [30]. Each analysis incorporated a background acquisition of approximately 20–30 s followed by 50 s of data acquisition from the sample. An Excel-based software ICPMSDataCal was used to perform off-line selection and integration of background and analyzed signals, time-drift correction and quantitative calibration for trace element analysis [30].

3.3. Bulk Techniques

Clean orthopyroxene grains were ground to powder and analyzed using X-Ray powder diffraction (XRD) for purity, X-ray fluorescence (XRF) spectrometry for major elements and solution ICP-MS for trace elements, respectively.

(IGCEA-XRD) Purity of MK-1 orthopyroxene powder was investigated by collecting its XRD patterns using a D8 Advance X-ray diffractometer (Bruker Scientific Instruments Hong Kong Company, China) (40 kV and 40 mA) in the 2θ range of 10° to 60° at the Institute of Geology, China Earthquake Administration (IGCEA).

(IGGCAS-XRF) Major element data of bulk orthopyroxene samples were obtained by XRF spectrometry on fused glass discs using a PANalytical AXIOS Minerals instrument (PANalytical B.V., Almelo, Holland) at the Rock-Mineral Preparation and Analysis Lab, IGGCAS. The PANalytical AXIOS Minerals equipped with a Rh anode X-ray tube and 4 kW excitation power is a sequential instrument with a single goniometer based measuring channel covering the complete elemental measurement range from F to U in the concentration range from 1.0 g g^{-1} to % level, determined in vacuum media [31]. Glass discs for WD-XRF analysis were prepared via the fusion of 0.6 g of the standard sample with 6.0 g of lithium tetraborate: metaborate (2:1) (Lithium borates 67–33, Claisse, Canada), using Pt-Au crucibles and molds employing electric fusion equipment (Claisse Fluxy, Corporation Scientific Claisse Inc., Quebec, Canada) [32]. Each disc was analyzed fifteen times, and greater variability between discs was seen than between repeated measurements with the $\text{RSD} < 1\%$ for all elements that were $> 0.1\%$ oxide in mass fraction.

(CAGS-XRF) Major and trace elements of bulk orthopyroxene samples were also measured on XRF (Primus II, Rigaku, Tokyo, Japan) at the National Research Center (NRC), Chinese Academy of Geological Sciences (CAGS), Beijing. The detailed sample-digesting procedure was as follows: (1) Sample powder (200 mesh) was placed in an oven at 105°C to dry for 12 h; (2) $\sim 1.0 \text{ g}$ dried sample was accurately weighted and placed in the ceramic crucible and then heated in a muffle furnace at 1000°C for 2 h. After cooling to 400°C , this sample was placed in the drying vessel and weighted again in order to calculate the loss on ignition (LOI); and (3) 0.6 g sample powder was mixed with 6.0 g cosolvent ($\text{Li}_2\text{B}_4\text{O}_7\text{:LiBO}_2\text{:LiF} = 9\text{:}2\text{:}1$) and 0.3 g oxidant (NH_4NO_3) in a Pt crucible, which was

placed in the furnace at 1150 °C for 14 min. Then, this melting sample was quenched with air for 1 min to produce flat discs on the fire brick for the XRF analyses. The analytical uncertainties of major elements were within 5%.

(CAGS—Solution ICP-MS) Trace element analysis of bulk orthopyroxene samples was conducted on Agilent 7700 e ICP-MS (Agilent Technologies, Palo Alto, California, USA) at NRC, CAGS. The detailed sample-digesting procedure was as follows: (1) Orthopyroxene powder (200 mesh) was placed in an oven at 105 °C to dry for 12 h; (2) 50 mg sample powder was accurately weighed and placed in a Teflon bomb; (3) 1 mL HNO₃ and 1 mL HF were slowly added into the Teflon bomb; (4) Teflon bomb was put in a stainless steel pressure jacket and heated to 190 °C in an oven for >24 h; (5) after cooling, the Teflon bomb was opened and placed on a hotplate at 140 °C and evaporated to incipient dryness, and then 1 mL HNO₃ was added and evaporated to dryness again; (6) 1 mL of HNO₃, 1 mL of MQ water and 1 ml internal standard solution of 1 µg g⁻¹ were added, and the Teflon bomb was resealed and placed in the oven at 190 °C for >12 h; (7) the final solution was transferred to a polyethylene bottle and diluted to 100 g by the addition of 2% HNO₃. The analytical uncertainties were within 10% for elements with abundances <10 µg g⁻¹, and approximately 5% for those >10 µg g⁻¹.

4. Results and Discussion

4.1. Homogeneity Evaluation

The homogeneity of major and trace elements is a fundamental requirement of any reference material [20,33–35]. In order to test the homogeneity of the orthopyroxene grains, eleven core-to-rim profiles (220 spots) were carried out by EPMA, and twelve core-to-rim profiles (240 spots) were carried out using LA-ICPMS by two institutions (Figure 1). Tables in this study list all analytical results provided by each laboratory, including major and trace elements mass fractions, mean values, standard deviation of mean (SE), relative deviation of mean (RSE), and relative standard deviations (RSD), displaying the dispersion of the data. Figures 2–6 show EPMA and LA-ICPMS mass fraction data of the profiles measured for the studied samples.

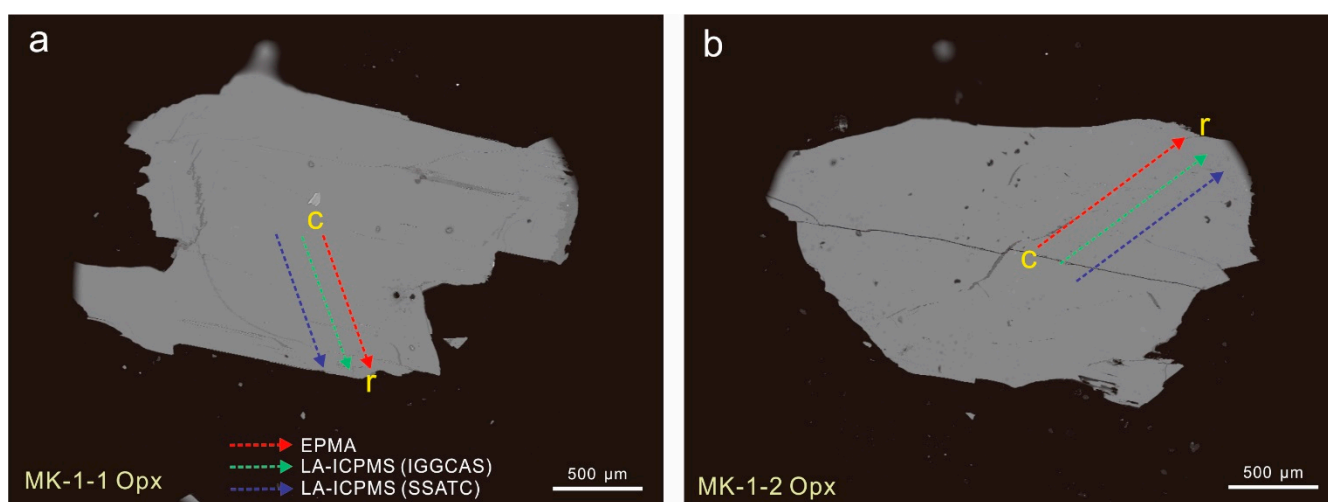


Figure 1. Representative backscatter electron (BSE) images of MK-1 orthopyroxene. (a), MK-1-1; (b), MK-1-2. The red lines show the core-to-rim profiles of EPMA analyzed spots, the green lines represent LA-ICPMS analyzed spots obtained from IGGCAS, and the purple lines represent LA-ICPMS analyzed spots obtained from SSATC.

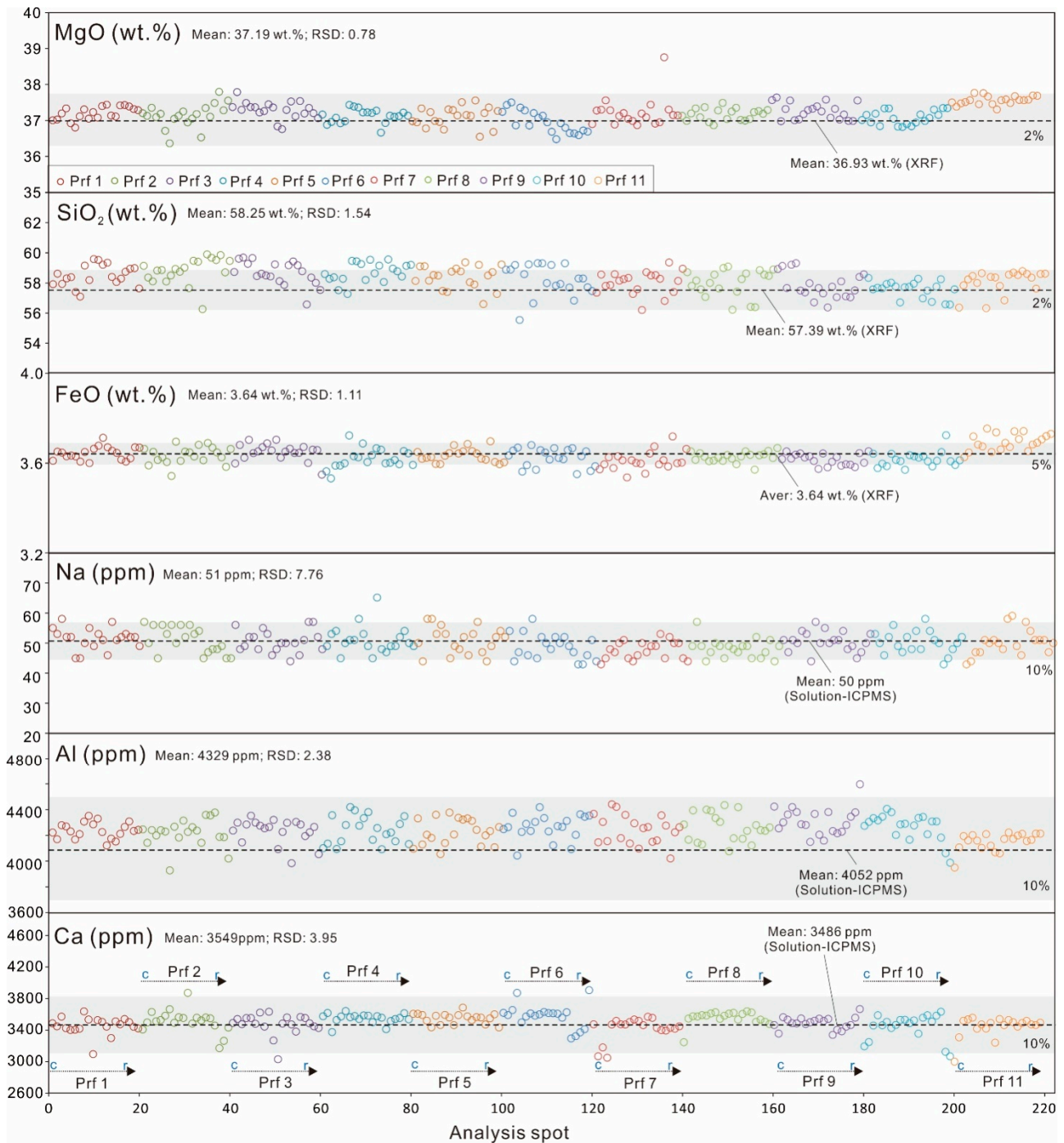


Figure 2. Core-to-rim chemical profiles using EPMA for MgO, SiO₂, FeO, Na, Al, and Ca for MK-1 orthopyroxene. The relative standard deviations (RSD) display the dispersion of the data. The dotted line represents the mean value obtained by XRF or solution-ICPMS. Light shaded area represents 2% to 20% of variation from the mean. Prf1 profile 1.

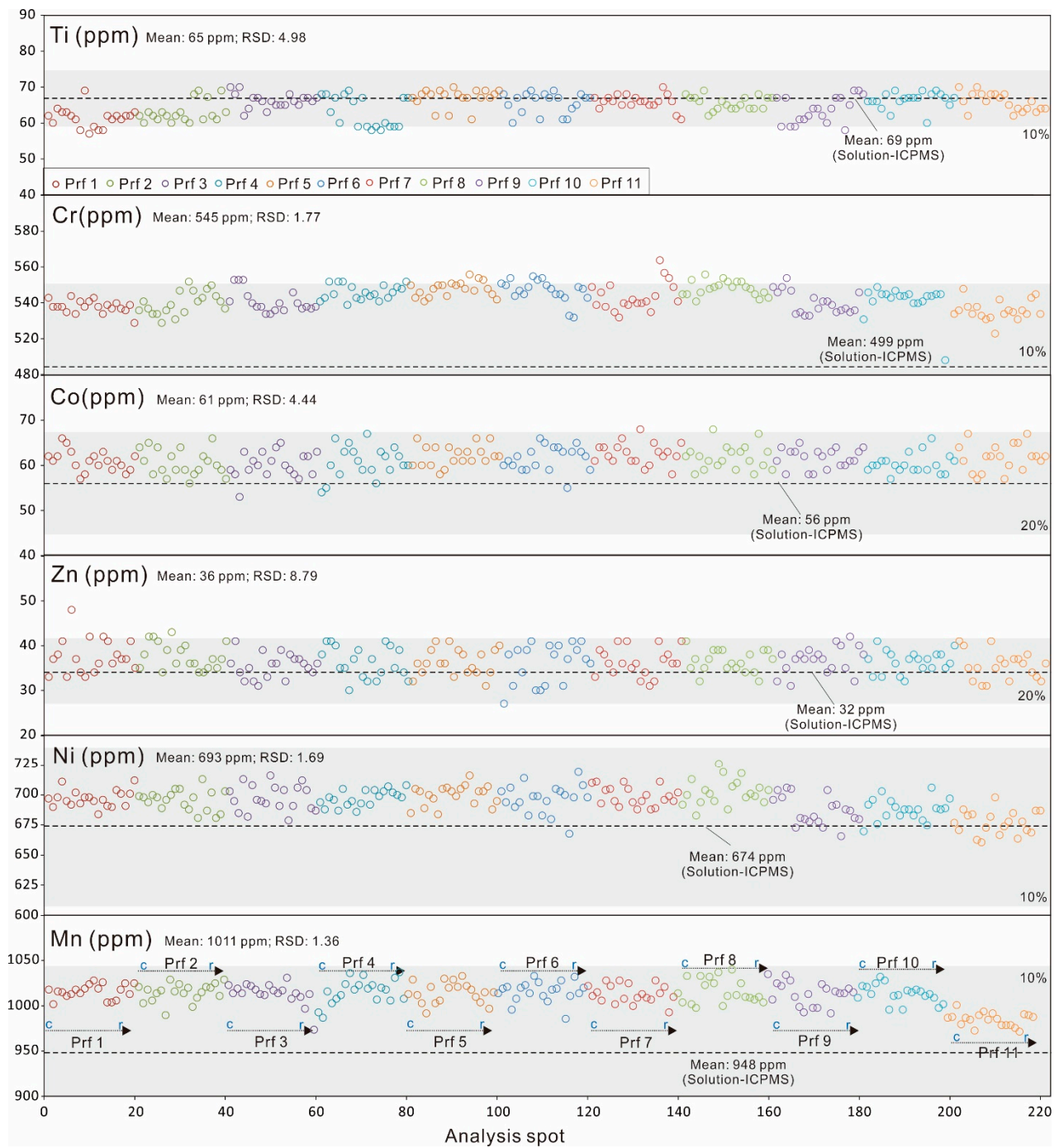


Figure 3. Core-to-rim chemical profiles using EPMA for Ti, Cr, Co, Zn, Ni, and Mn for MK-1 orthopyroxene. For details see caption of Figure 2.

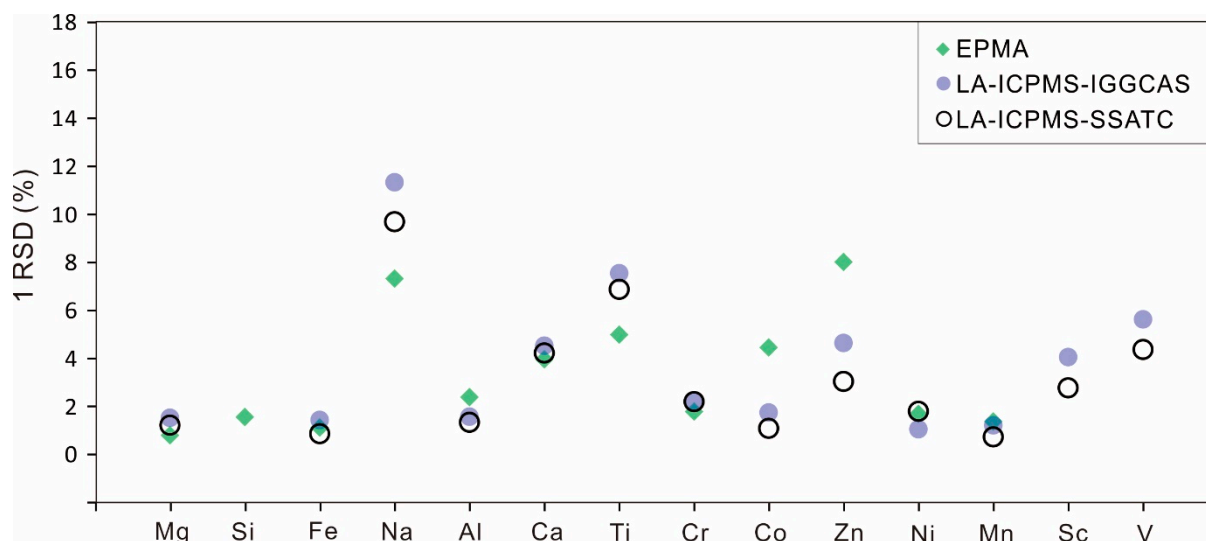


Figure 4. EPMA and LA-ICPMS homogeneous data for MK-1 orthopyroxene. The relative standard deviations (RSDs) display the dispersion of the data.

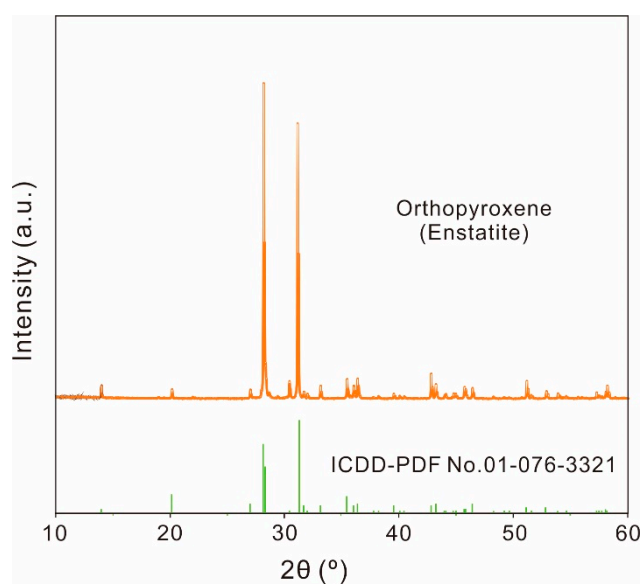


Figure 5. XRD patterns of orthopyroxene obtained via two routes.

Eleven orthopyroxene grains were shown by extensive EPMA data to have low within-sample variations in terms of major elements and most trace elements, indicating the homogeneous compositions in individual samples (Supplemental Table S1). MK-1 orthopyroxene has MgO content in the range from 36.2 to 38.8 wt.% with the mean of 37.2 wt.%, SiO₂ content in the range from 55.5 to 59.9 wt.% with the mean of 58.3 wt.%, and FeO content in the range from 3.76 to 5.54 wt.% with the mean of 3.64 wt.%. It has high concentrations of Al (4329 $\mu\text{g g}^{-1}$), Ca (3549 $\mu\text{g g}^{-1}$), Cr (545 $\mu\text{g g}^{-1}$), Ni (693 $\mu\text{g g}^{-1}$), and Mn (1011 $\mu\text{g g}^{-1}$). The contents of Na, Ti, Co, and Zn range from 44 to 66 $\mu\text{g g}^{-1}$, 57 to 70 $\mu\text{g g}^{-1}$, 53 to 68 $\mu\text{g g}^{-1}$, and 27 to 48 $\mu\text{g g}^{-1}$, respectively.

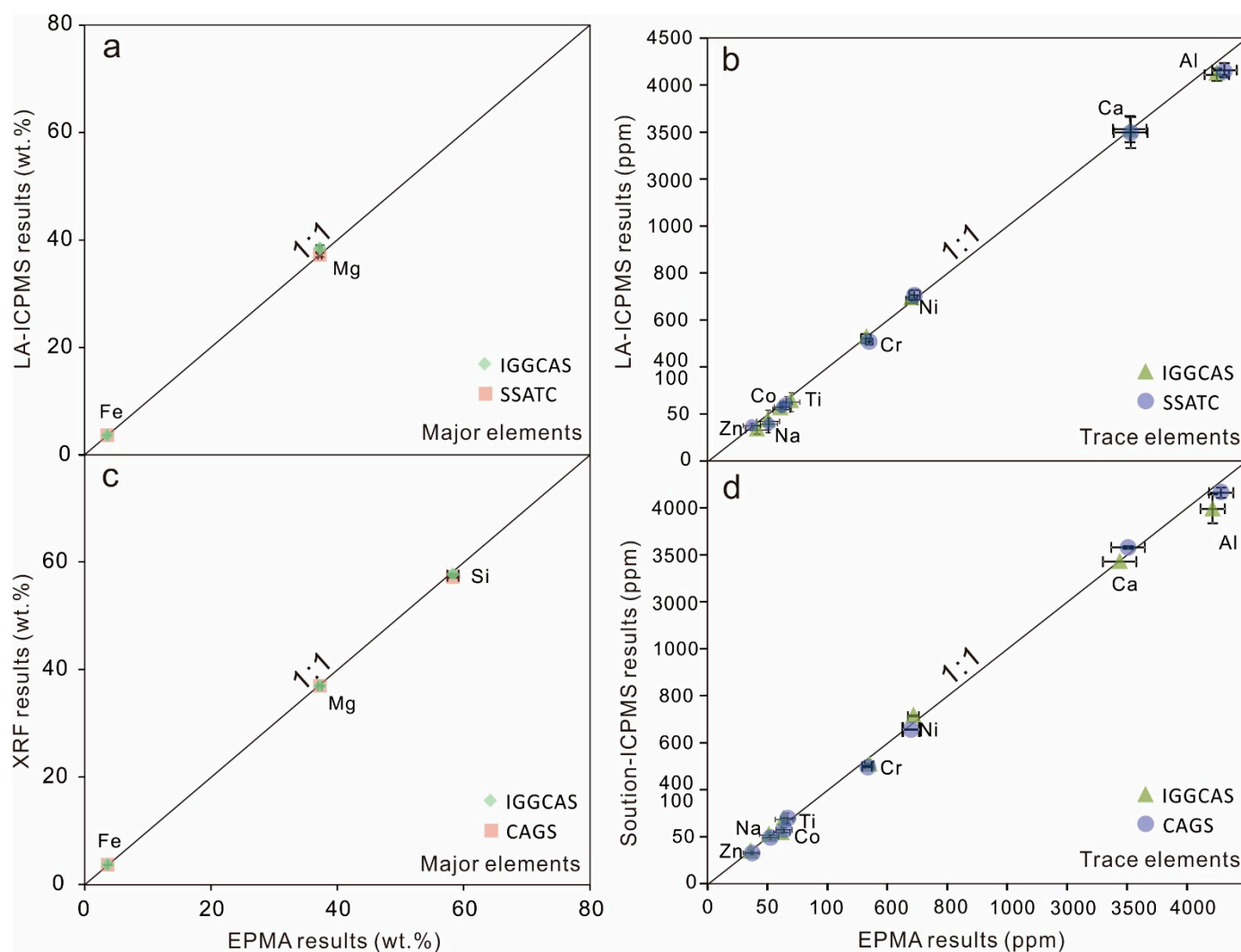


Figure 6. Comparison of major and trace element abundances determined by EPMA, LA-ICPMS, XRF, and solution-ICPMS techniques. A 1:1 line is drawn in each plot for comparison purposes. EPMA data show outstanding agreements with XRF and LA-ICPMS results obtained by different laboratories with RSE $< \pm 2\%$ for major elements (a,c) and with RSE $< \pm 10\%$ for trace elements (b,d).

As shown in Figure 2, all EPMA results of MK-1 orthopyroxene show that the major elements (Mg, Si, Fe) are homogeneous within $\pm 2\%$ (1σ RSD). Aluminum, Ca, Ti, Cr, Co, Ni, and Mn are also homogeneous with RSD $< \pm 5\%$, whereas Na and Zn yield the RSD values of $\pm 7.76\%$ and $\pm 8.79\%$, respectively (Figure 3). The trace elements were also determined with the LA-ICPMS technique, which are considered as best estimated for accurate mass fractions. As shown in Figure 4, the data from IGGCAS laboratory suggest that Al, Ca, Cr, Co, Zn, Ni, Mn, and Sc variations are within $\pm 5\%$ (Figure 4, Supplemental Table S2). Sodium shows the highest variation in MK-1 orthopyroxene ($\pm 12.94\%$). Vanadium and Ti variations are within $\pm 5.91\%$ and $\pm 7.93\%$. The LA-ICPMS data from SSACT laboratory have similar trace elements results. Aluminum, Ca, Cr, Co, Zn, Ni, Mn, Sc, and V are homogeneous with RSD $< \pm 5\%$, except for Na and Ti ($\pm 9.32\%$ and $\pm 7.28\%$, respectively). Therefore, MK-1 orthopyroxene can be regarded as homogeneous for the investigated major and trace elements within measurement uncertainties, and has high potential to be used as a reference material for in-situ microanalysis.

4.2. Comparison of Techniques and Recommended Values

The comparison of all mass fraction data obtained by the different applied techniques is graphically displayed on the chemical profiles presented in Figures 2–6. In total, eleven core-to-rim profiles were carried out by EPMA, twelve core-to-rim profiles were carried out using LA-ICPMS by two institutions, one aliquot was carried out by XRD, and five aliquots were analyzed by solution-ICPMS and five aliquots by XRF by two institutions. The consistency of the data obtained in different laboratories by different analytical techniques is considered a measure of data quality.

The XRD analysis was carried out to verify the purity of the orthopyroxene powder. The results show that only enstatite signal was shown in Figure 5, indicating that there is no pollution of other minerals. Therefore, the studied orthopyroxene powder is pure enough to prepare the XRF and solution-ICPMS.

Three different mass fraction measurements were obtained for major elements (Mg, Si, Fe) using four independent techniques. EPMA data show outstanding agreements with XRF and LA-ICPMS data obtained by different laboratories with RSE < ±2% (Figure 6).

For Al, Ca, Co, Cr, Zn, Mn, and Ni, EPMA and LA-ICPMS data show good agreements (RSE < ±5%). Mass fractions of Ti obtained by EPMA and LA-ICPMS agree within ±7%. For Na, the comparison of techniques must be performed cautiously as the mass fractions obtained by EPMA are higher than those obtained by LA-ICPMS, which is probably due to different matrix correction methods. Relative error (RE) was used to compare the consistency between EPMA and solution-ICPMS data (Supplemental Table S3). The data from both techniques are also consistent with RE not exceeding ±10% (1σ). The above results suggest that the mass fractions of major and trace elements in MK-1 orthopyroxene obtained by different techniques and laboratories are almost identical, showing an outstanding agreement. The recommended reference values are shown in Table 2.

Table 2. Summary of all MK-1 orthopyroxene analyses.

| Comment | Major Elements (wt.%) | | | | Trace Elements (ppm) | | | | | | | | | | |
|-----------------------|--------------------------------|------------------|------|------|----------------------|------|------|------|------|------|------|------|------|------|------|
| | MgO | SiO ₂ | FeO | Na | Al | Ca | Ti | Cr | Co | Zn | Ni | Mn | Sc | V | |
| MK-1 orthopyroxene | EPMA-IGGCAS (220 analyses) | | | | | | | | | | | | | | |
| | Mean | 37.2 | 58.2 | 3.64 | 51 | 4329 | 3549 | 65 | 545 | 61 | 36 | 693 | 1011 | | |
| | 1 σ | 0.29 | 0.86 | 0.04 | 4 | 103 | 140 | 3 | 10 | 3 | 3 | 12 | 14 | | |
| | RSD | 0.78 | 1.48 | 1.11 | 7.76 | 2.38 | 3.95 | 4.98 | 1.77 | 4.44 | 8.79 | 1.69 | 1.36 | | |
| | LA-ICPMS-IGGCAS (120 analyses) | | | | | | | | | | | | | | |
| | Mean | 38.4 | 58.2 | 3.66 | 42 | 4109 | 3531 | 62 | 517 | 55 | 38 | 677 | 923 | 7 | 15 |
| | 1 σ | 0.56 | 0.0 | 0.05 | 5 | 71 | 184 | 5 | 11 | 1 | 2 | 9 | 12 | 0 | 1 |
| | RSD | 1.45 | 0.00 | 1.43 | 11.1 | 1.72 | 5.20 | 7.75 | 2.15 | 1.86 | 4.53 | 1.28 | 1.32 | 5.66 | 4.13 |
| | LA-ICPMS-SSATC (120 analyses) | | | | | | | | | | | | | | |
| | Mean | 37.9 | 58.2 | 41 | 4149 | 3492 | 62 | 505 | 57 | 37 | 668 | 940 | 7 | 14 | 41 |
| | 1 σ | 0.50 | 0.0 | 4 | 70 | 174 | 4 | 11 | 1 | 1 | 13 | 8 | 0 | 0 | 4 |
| | RSD | 1.33 | 0.00 | 9.71 | 1.70 | 4.97 | 7.02 | 2.17 | 1.06 | 3.07 | 1.92 | 0.88 | 4.45 | 2.78 | 9.71 |
| | Bulk-IGGCAS (2 analyses) | | | | | | | | | | | | | | |
| | Mean | 36.9 | 57.7 | 3.67 | 54.0 | 3959 | 3406 | 70.1 | 500 | 55.8 | 32.9 | 705 | 939 | 14.7 | 9.16 |
| | 1 σ | 0.08 | 0.14 | 0.01 | 1.39 | 151 | 0.00 | 0.85 | 3.54 | 0.23 | 0.42 | 1.84 | 2.74 | 0.09 | 0.08 |
| | Bulk-CAGS (3 analyses) | | | | | | | | | | | | | | |
| | Mean | 36.9 | 57.2 | 3.62 | 49.0 | 4114 | 3540 | 68.5 | 499 | 56.4 | 32.8 | 654 | 955 | 14.9 | 9.00 |
| | 1 σ | 0.04 | 0.13 | 0.01 | 1.29 | 54.1 | 14.9 | 2.95 | 1.85 | 0.98 | 1.03 | 6.90 | 11.8 | 0.13 | 0.39 |
| Recommended values | Mean | 37.3 | 57.8 | 3.66 | 46.4 | 4111 | 3486 | 64.7 | 513 | 56.6 | 34.6 | 684 | 950 | 14.7 | 7.96 |
| | 1 σ | 0.61 | 0.49 | 0.03 | 7.08 | 137 | 59.9 | 4.77 | 20.0 | 3.09 | 2.01 | 19.3 | 38.3 | 0.43 | 1.30 |

Table 2. Cont.

| Comment | | Major Elements (wt.%) | | | | | Trace Elements (ppm) | | | | | | | |
|------------------------------|-----|-----------------------|------------------|-------|-------|------|----------------------|-------|------|------|------|-------|------|----|
| | | MgO | SiO ₂ | FeO | Na | Al | Ca | Ti | Cr | Co | Zn | Ni | Mn | Sc |
| EPMA, LA-ICPMS- IGGCAS | SE | 0.62 | 0.00 | 0.05 | 5.03 | 63.3 | 138 | 4.38 | 11.4 | 0.92 | 1.56 | 7.21 | 11.1 | |
| | RSE | 1.68 | 0.00 | 1.30 | 9.73 | 1.46 | 3.85 | 6.80 | 2.09 | 1.50 | 4.27 | 1.04 | 1.09 | |
| EPMA, LA- ICPMS-SSATC | SE | 0.37 | 0.00 | 0.04 | 3.65 | 74.9 | 165 | 4.47 | 11.0 | 0.63 | 1.12 | 13.1 | 6.83 | |
| | RSE | 1.00 | 0.00 | 0.97 | 7.06 | 1.73 | 4.61 | 6.95 | 2.02 | 1.04 | 3.07 | 1.88 | 0.67 | |
| EPMA, Bulk IGGCAS | RE | 0.68 | 0.93 | −0.77 | −5.77 | 8.54 | 4.04 | −8.06 | 8.32 | 8.90 | 9.71 | −1.67 | 7.13 | |
| EPMA, Bulk CAGS | RE | 0.72 | 1.79 | 0.45 | 4.13 | 4.97 | 0.25 | −5.60 | 8.45 | 8.01 | 9.97 | 5.68 | 5.54 | |

σ , standard deviation; RSD, relative standard deviation; SE, standard deviation of mean (standard error); RSE, relative standard deviation of mean; RE, relative error.

Metrological traceability is a key concept in the characterization of reference materials. Traceability in this study was established by the use of standard solutions and international reference materials. For example, the standard solutions for making calibration curves for ICP-OES analysis were prepared from NIST calibration standard solutions, and the experimental equipment, scales and measuring instruments were regularly verified or calibrated by certified reference materials. Solid international reference materials were used to establish the traceability of the EPMA and LA-ICP-MS techniques. Meanwhile, all the collaborating laboratories have demonstrated their technical competence in geochemical analytical research, typically by the publications of reports and research papers describing their metrological traceability.

5. Conclusions

The grains of natural orthopyroxene (MK-1) separated from an ultramafic intrusion at the Mogok metamorphic belt are sufficiently homogeneous and thus highly suitable as reference material for in-situ mass fraction measurement of orthopyroxene by EPMA, LA-ICPMS, and SIMS. Eleven core-to-rim profiles were carried out by EPMA, twelve core-to-rim profiles were carried out using LA-ICPMS, and five aliquots were analyzed by solution-ICPMS and five aliquots by XRF in five different analytical laboratories. Well-characterized reference values were obtained for major elements (Mg, Si, Fe) and trace elements (Na, Al, Ca, Ti, Cr, Co, Zn, Ni, Mn, Sc, and V), which can be used for mass fraction measurement of unknown orthopyroxene by microbeam techniques for quality control and method validation purposes.

MK-1 orthopyroxene may be valuable for in-situ microanalysis work, we are willing to distribute grains of MK-1 orthopyroxene to the scientific community upon request (e-mail address: jjalihu@mail.iggcas.ac.cn).

Supplementary Materials: The following are available online at <https://www.mdpi.com/article/10.3390/min11121321/s1>, Supplemental Table S1: Compositions of major and trace elements of MK-1 orthopyroxene determined by EPMA; Supplemental Table S2: Compositions of major and trace elements of MK-1 orthopyroxene determined by LA-ICPMS; Supplemental Table S3: Bulk major and trace elements of MK-1 orthopyroxene determined by XRF and solution-ICPMS.

Author Contributions: Conceptualization, L.J.; methodology, Q.M., S.W., L.H., D.Z. and J.Y.; software, S.W., L.H. and J.Y.; validation, L.J. and Y.C.; formal analysis, B.S.; investigation, L.J.; resources, Y.C.; data curation, Q.M.; writing—original draft preparation, L.J.; writing—review and editing, L.J., B.S., and Y.C.; funding acquisition, L.J. All authors have read and agreed to the published version of the manuscript.

Funding: This research was funded by the National Natural Science Foundation of China, grant number 42002096 and 41822202 and Experimental Technology Innovation Fund of the Institute of Geology and Geophysics, Chinese Academy of Sciences [E1518506].

Informed Consent Statement: Informed consent was obtained from all subjects involved in the study.

Data Availability Statement: The data presented in this study are available within the article.

Acknowledgments: The authors thank Si Chen and Yibing Li for field sampling work. We are also grateful to the anonymous reviewers for their constructive comments. This study was financially supported by the National Natural Science Foundation of China (No. 42002096, 41822202) and Experimental Technology Innovation Fund of the Institute of Geology and Geophysics, Chinese Academy of Sciences [E1518506].

Conflicts of Interest: The authors declare no conflict of interest. The funders had no role in the design of the study; in the collection, analyses, or interpretation of data; in the writing of the manuscript, or in the decision to publish the results.

References

1. Nixon, P.H. *Mantle Xenoliths*; John Wiley and Sons: Hoboken, NJ, USA, 1987; p. 844.
2. Sisson, T.W. Pyroxene-high silica rhyolite trace element partition coefficients measured by ion microprobe. *Geochim. Cosmochim. Acta* **1991**, *55*, 1575–1585. [[CrossRef](#)]
3. Blatter, D.L.; Carmichael, I.S.E. Hydrous phase equilibria of a Mexican high-silica andesite: A candidate for a mantle origin? *Geochim. Cosmochim. Acta* **2001**, *65*, 4043–4065. [[CrossRef](#)]
4. Longhi, J. Some phase equilibrium systematics of lherzolite melting: I. *Geochem. Geophys. Geosyst.* **2002**, *3*, 1–33. [[CrossRef](#)]
5. Cawthorn, R.G. *Layered Intrusions*; Elsevier Science Publishers BvS: Amsterdam, The Netherlands, 1996; Volume 15, p. 531.
6. Schroetter, J.M.; Page, P.; Bedard, J.H.; Tremblay, A.; Becu, V. Forearc extension and seafloor spreading in the Thetford Mines Ophiolite Complex. In *Ophiolites in Earth History*; Dilek, Y., Robinson, P.T., Eds.; The Geological Society: London, UK, 2004; Volume 218, pp. 231–251.
7. Bédard, J.H. Trace element partitioning coefficients between silicate melts and orthopyroxene: Parameterizations of D variations. *Chem. Geol.* **2007**, *244*, 263–303. [[CrossRef](#)]
8. Barnes, S.J.; Mole, D.R.; Le Vaillant, M.; Campbell, M.J.; Verrall, M.R.; Roberts, M.P. Poikilitic textures, heteradcumulates and zoned orthopyroxenes in the Ntaka Ultramafic Complex, Tanzania: Implications for crystallization mechanisms of oikocrysts. *J. Petrol.* **2016**, *57*, 1171–1198. [[CrossRef](#)]
9. Wang, K.Y.; Song, X.Y.; Yi, J.N.; Barnes, S.J.; She, Y.W.; Zheng, W.Q.; Schoneveld, L.E. Zoned orthopyroxenes in the Ni-Co sulfide ore-bearing Xiarihamu mafic-ultramafic intrusion in northern Tibetan Plateau, China: Implications for multiple magma replenishments. *Ore Geol. Rev.* **2019**, *113*, 103082. [[CrossRef](#)]
10. Kinman, W.S.; Neal, C.R. Magma evolution revealed by anorthite-rich plagioclase cumulate xenoliths from the Ontong Java Plateau: Insights into LIP magma dynamics and melt evolution. *J. Volcanol. Geoth. Res.* **2006**, *154*, 131–157. [[CrossRef](#)]
11. Saunders, K.; Rinnen, S.; Blundy, J.; Dohmen, R.; Klemme, S.; Arlinghaus, H.F. TOF-SIMS and electron microprobe investigations of zoned magmatic orthopyroxenes: First results of trace and minor element analysis with implications for diffusion modeling. *Am. Miner.* **2012**, *97*, 532–542. [[CrossRef](#)]
12. Elardo, S.M.; Shearer, C.K., Jr. Magma chamber dynamics recorded by oscillatory zoning in pyroxene and olivine phenocrysts in basaltic lunar meteorite Northwest Africa 032. *Am. Miner.* **2014**, *99*, 355–368. [[CrossRef](#)]
13. Ubide, T.; Kamber, B.S. Volcanic crystals as time capsules of eruption history. *Nat. Commun.* **2018**, *9*, 326. [[CrossRef](#)]
14. Ginibre, C.; Kronz, A.; Woerner, G. High-resolution quantitative imaging of plagioclase composition using accumulated backscattered electron images: New constraints on oscillatory zoning. *Contrib. Mineral. Petrol.* **2002**, *142*, 436–448. [[CrossRef](#)]
15. Page, P.; Barnes, S.J. Using trace elements in chromites to constrain the origin of podiform chromitites in the Thetford Mines ophiolite, Quebec, Canada. *Econ. Geol.* **2009**, *104*, 997–1018. [[CrossRef](#)]
16. Bai, Y.; Su, B.X.; Xiao, Y.; Lenaz, D.; Asamoah Sakyi, P.; Liang, Z.; Chen, C.; Yang, S.H. Origin of reverse zoned Cr-spinels from the Paleoproterozoic Yanmenguan mafic-ultramafic complex in the North China Craton. *Minerals* **2018**, *8*, 62. [[CrossRef](#)]
17. Taylor, W.R. An experimental test of some geothermometer and geobarometer formulations for upper mantle peridotites with application to the thermobarometry of fertile lherzolites and garnet websterite. *Neues Jahrb. Für Mineral. Abh.* **1998**, *172*, 381–408.
18. Bertrand, P.; Sotin, C.; Mercier, J.C.C.; Takahashi, E. From the simplest chemical system to the natural one: Garnet peridotite barometry. *Contrib. Mineral. Petrol.* **1986**, *93*, 168–178. [[CrossRef](#)]
19. Brey, G.P.; Bulatov, V.K.; Gurnis, A.V. Geobarometry for peridotites: Experiments in simple and natural systems from 6 to 10 GPa. *J. Petrol.* **2008**, *49*, 3–24. [[CrossRef](#)]
20. Batanova, V.G.; Thompson, J.M.; Danyushevsky, L.V.; Portnyagin, M.V.; Garbe-Schonberg, D.; Hauri, E.; Kimura, J.I.; Chang, Q.; Senda, R.; Goemann, K.; et al. New olivine reference material of In situ microanalysis. *Geostand. Geoanalytical Res.* **2019**, *43*, 453–473. [[CrossRef](#)]

21. Su, B.; Chen, Y.; Mao, Q.; Zhang, D.; Jia, L.H.; Guo, S. Minor elements in olivine inspect the petrogenesis. *Lithos* **2019**, *344–345*, 207–216. [[CrossRef](#)]
22. Pankhurst, M.J.; Walshaw, R.; Morgan, D. Major element chemical heterogeneity in Geo 2 olivine microbeam reference material: A spatical approach to quantifying heterogeneity in primary reference materials. *Geostand. Geoanalytical Res.* **2017**, *41*, 85–91. [[CrossRef](#)]
23. Armstrong, J.T. Citzaf-a package of correction programs for the quantitative electron microbeam X-ray-analysis of thick polished materials, thin-films, and particles. *Microbeam Analasis* **1995**, *4*, 177–200.
24. Wu, S.T.; Worner, G.; Jochum, K.P.; Stoll, B.; Simon, K.; Kronz, A. The Preparation and Preliminary Characterisation of Three Synthetic Andesite Reference Glass Materials (ARM-1, ARM-2, ARM-3) for In Situ Microanalysis. *Geostand. Geoanal. Res.* **2019**, *43*, 567–584. [[CrossRef](#)]
25. Griffin, W.L.; Powell, W.; Pearson, N.J.; O'Reilly, S.Y. *GLITTER: Data Reduction Software for Laser Ablation ICP-MS*; Mineralogical Association of Canada: Quebec, QC, Canada, 2008; Volume 40, pp. 308–311.
26. Xie, L.W.; Zhang, Y.B.; Zhang, H.H.; Sun, J.F.; Wu, F.Y. In situ simultaneous determination of trace elements, U-Pb and Lu-Hf isotopes in zircon and baddeleyite. *Chin. Sci. Bull.* **2008**, *53*, 1565–1573. [[CrossRef](#)]
27. Wu, S.T.; Karius, V.; Schmidt, B.C.; Simon, K.; Woerner, G. Comparison of Ultrafine Powder Pellet and Flux-free Fusion Glass for Bulk Analysis of Granitoids by Laser Ablation-Inductively Coupled Plasma-Mass Spectrometry. *Geostand. Geoanal. Res.* **2018**, *42*, 575–591. [[CrossRef](#)]
28. Zong, K.Q.; Klemm, R.; Yuan, Y.; He, Z.Y.; Guo, J.L.; Shi, X.L.; Liu, Y.S.; Hu, Z.C.; Zhang, Z.M. The assembly of Rodinia: The correlation of early Neoproterozoic (ca. 900 Ma) high-grade metamorphism and continental arc formation in the southern Beishan Orogen, southern Central Asian Orogenic Belt (CAOB). *Precambrian Res.* **2017**, *290*, 32–48. [[CrossRef](#)]
29. Hu, Z.C.; Zhang, W.; Liu, Y.S.; Gao, S.; Li, M.; Zong, K.Q.; Chen, H.H.; Hu, S.H. “Wave” Signal-Smoothing and Mercury-Removing Device for Laser Ablation Quadrupole and Multiple Collector ICPMS Analysis: Application to Lead Isotope Analysis. *Anal. Chem.* **2015**, *87*, 1152–1157. [[CrossRef](#)] [[PubMed](#)]
30. Liu, Y.S.; Hu, Z.C.; Gao, S.; Günther, D.; Xu, J.; Gao, C.G.; Chen, H.H. In situ analysis of major and trace elements of anhydrous minerals by LA-ICP-MS without applying an internal standard. *Chem. Geol.* **2008**, *257*, 34–43. [[CrossRef](#)]
31. Xue, D.S.; Su, B.X.; Zhang, D.P.; Liu, Y.H.; Guo, J.J.; Guo, Q.; Sun, J.F.; Zhang, S.Y. Quantitative verification of 1:100 diluted fused glass beads for X-ray fluorescence analysis of geological specimens. *J. Anal. At. Spectrom.* **2020**, *35*, 2826–2833. [[CrossRef](#)]
32. Zhang, D.P.; Xue, D.S.; Liu, Y.H.; Wan, B.; Guo, Q.; Guo, J.J. Comparative Study of Three Mixing Methods in Fusion Technique for Determining Major and Minor Elements Using Wavelength Dispersive X-ray Fluorescence Spectroscopy. *Sensors* **2020**, *18*, 5325. [[CrossRef](#)]
33. Potts, P.J.; Tindle, A.G.; Isaacs, M.C. On the precision of electron-microprobe data—A new test for the homogeneity of mineral standards. *Am. Mineralogist.* **1983**, *68*, 1237–1242.
34. Jochum, K.P.; Dingwell, D.B.; Rocholl, A.; Stoll, B.; Hofmann, A.W.; Becher, S.; Besmehn, A.; Bessette, D.; Dietze, H.J.; Dulski, P.; et al. The preparation and preliminary characterization of eight geological MPI-DING reference glasses for in-situ microanalysis. *Geostand. Newsl. J. Geostand. Geoanal.* **2000**, *24*, 87–133. [[CrossRef](#)]
35. Harries, D. Homogeneity testing of microanalytical reference materials by electron probe microanalysis (EPMA). *Chem. Erde–Geochem.* **2014**, *74*, 375–384. [[CrossRef](#)]